Eur. Phys. J. A **9**, 357–364 (2000)

THE EUROPEAN PHYSICAL JOURNAL A

Thermal dileptons from quark and hadron phases of an expanding fireball

R.A. Schneider[a] and W. Weise

Physik-Department, Technische Universität München,D-85747 Garching, Germany

Received: 4 August 2000
Communicated by A. Schäfer

Abstract. A fireball model with time evolution based on transport calculations is used to examine the dilepton emission rate of an ultra-relativistic heavy-ion collision. A transition from hadronic matter to a quark-gluon plasma at a critical temperature T_C between 130–170 MeV is assumed. We also consider a possible mixed phase scenario. We include thermal corrections to the hadronic spectra below T_C and use perturbation theory above T_C. The sensitivity of the spectra with respect to the freeze-out temperature, the initial fireball temperature and the critical temperature is investigated.

PACS. 12.38.Mh Quark-gluon plasma – 11.10.Wx Finite-temperature field theory

1 Introduction

There are convincing arguments that the theory of the strong interaction, QCD, exhibits a phase transition at sufficiently high temperatures from a confined hadronic phase to the quark-gluon plasma (QGP) phase [1–3]. Lattice QCD results set the critical temperature T_C to about 150–200 MeV [4–6]. It is hoped that it is possible to create the QGP in ultrarelativistic heavy-ion collisions at CERN and BNL, and there are preliminary indications that the QGP might have already been encountered [7–9].

Dileptons (e^+e^- or $\mu^+\mu^-$ pairs) are considered to be an optimal probe for the early stages of the collision because they leave the hot region without thermalization. Hadrons which reach the detector can only tell us about the later stage of the collision, the freeze-out zone. When the fireball created in a heavy-ion collision is in the QGP or partonic phase, dileptons are mainly produced by thermal quark-antiquark annihilation. As the system expands, it cools off and undergoes the transition into the hadronic phase. There, dileptons come mainly from pion and kaon annihilation processes, which are dynamically enhanced through the formation of light vector meson resonances (ρ, ω and ϕ with masses below 1.1 GeV). The dilepton emission rate is proportional to the imaginary part of the hadronic current-current correlation function, or the electromagnetic spectral function. The invariant mass distribution of the lepton pairs reflects the mass distributions of the vector mesons at the instant of decay. This offers the possibility to study the influence of finite temperature and baryonic density on the meson spectral distributions.

[a] e-mail: schneidr@ph.tum.de

In this paper, we calculate the purely thermal dilepton emission rate for both phases and compare it with data from the CERES/NA45 experiment. Much work has been done to interpret the observed dilepton enhancement in the low-mass region [7,10] in terms of in-medium modifications of hadron spectra [11–13]. We investigate the thermal modifications that the hadrons may exhibit in the limit of zero baryon density. We demonstrate that these alone can also explain the data very easily if the initial fireball temperature is sufficiently high to support a QGP during at least part of the expansion. Finally, we study the dependence of the shape of the dilepton emission spectra on the parameters of our simple fireball model and discuss a recently proposed mixed phase structure.

2 Dileptons from a fireball

The dilepton emission rate from a hot domain populated by particles in thermal equilibrium at temperature T is proportional to the imaginary part of the spin-averaged, time-like photon self-energy, with these particles as intermediate states. The thermally excited particles annihilate to yield a time-like virtual photon with four-momentum q which decays subsequently into a lepton-antilepton pair. The differential rate is given by

$$\frac{\mathrm{d}N}{\mathrm{d}^4x\mathrm{d}^4q} = \frac{\alpha^2}{\pi^3 q^2}\,\frac{1}{e^{\beta q^0}-1}\,\mathrm{Im}\bar{\Pi}(q,T), \qquad (1)$$

where $\alpha = e^2/4\pi$, $\beta = 1/T$, and we have neglected the lepton masses. We defined $\bar{\Pi}(q) = -\Pi^\mu_{\ \mu}/3$. Here $\Pi^\mu_{\ \mu}$ denotes the trace over the thermal photon self-energy which

is equivalent to the thermal current-current correlation function

$$\Pi_{\mu\nu}(q,T) = i \int \mathrm{d}^4x \; e^{iqx} \langle \mathcal{T} j_\mu(x) j_\nu(0) \rangle_\beta, \qquad (2)$$

where j_μ is the electromagnetic current. The result eq. (1) is valid to order α in the electromagnetic interaction and to all orders in the strong interaction.

To compare with experimental data, we set up a model for the space-time evolution of a heavy-ion collision, assuming approximate thermal equilibrium to be a useful concept [14]. Some recent discussions suggest [15,16] that equilibration times at the conditions of heavy-ion collisions at CERN may indeed be very short (less than 1 fm), small compared to expansion times of order 10 fm/c, although this is still a matter of debate. The easiest approach for our purposes is to use a simplified fireball model which parametrizes the time dependence of temperature and volume in accord with microscopic transport calculations [17,18]. This assumes that the fireball can be characterized by a homogeneous temperature at all times and that it cools off adiabatically with the parametrization

$$T(t) = (T^i - T^\infty) e^{-t/\tau_1} + T^\infty. \qquad (3)$$

This ansatz introduces the initial temperature T^i, a time constant τ_1 and an asymptotic temperature T^∞. Furthermore, we assume an isotropic expansion of the fireball in the centre-of-mass frame of the collision such that the time evolution of the volume can be described by

$$V(t) = \frac{N_B}{\rho(t)}, \qquad \rho(t) = \rho^i e^{-t/\tau_2}, \qquad (4)$$

where N_B is the number of baryons which participate in the reaction, τ_2 is another time constant and ρ^i is the initial baryon density of the hot spot. More sophisticated volume parametrizations can be used, but they introduce more parameters and the differences in the resulting integrated rates are marginal.

Finally, to obtain the measured dilepton rates, we integrate eq. (1) over the space-time history of the collision to compare them with the CERES/NA45 data. The CERES experiment is a *fixed-target* experiment, *i.e.* the dilepton rates are measured in the lab frame whereas our volume parametrization (4) is valid for a fireball at rest, in the c.m. frame of the collision. In the lab frame, the CERES detector covers a limited rapidity interval $\eta = 2.1$–2.65. The rapidity needed in order to boost to the c.m. frame is therefore 2.375. The CERES collaboration chose to display its data in the format $\mathrm{d}^2N/\mathrm{d}M\mathrm{d}\eta$, where η is the (pseudo-)rapidity of the virtual photon. The longitudinal momentum p_L is related to η by $p_\mathrm{L} = m_\mathrm{T} \sinh\eta$ with the "transverse mass" $m_\mathrm{T} = \sqrt{M^2 + p_\mathrm{T}^2}$. To be able to compare our calculated rates to the data, we integrate these rates over the transverse momentum p_T only, given that

$$\mathrm{d}^4p = M p_\mathrm{T} \; \mathrm{d}M \; \mathrm{d}\eta \; \mathrm{d}p_\mathrm{T} \; \mathrm{d}\theta.$$

This is equivalent to integrating over all three-momenta as long as we set $\eta = 0$ in the c.m. frame.

The formula for the space-time- and p_T-integrated dilepton rates is now

$$\frac{\mathrm{d}^2N}{\mathrm{d}M\mathrm{d}\eta} = 2\pi M \int_0^{t_\mathrm{f}} \mathrm{d}t \frac{N_B}{\rho(t)} \int_0^\infty \mathrm{d}p_\mathrm{T} p_\mathrm{T} \times \frac{\mathrm{d}N(T(t), M, \eta, p_\mathrm{T})}{\mathrm{d}^4x \mathrm{d}^4p} \; \mathrm{Acc}(M, \eta, p_\mathrm{T}), \qquad (5)$$

where t_f is the freeze-out time of the collision, and the matrix $\mathrm{Acc}(M, \eta, p_\mathrm{T})$ accounts for the experimental acceptance cuts specific to the detector. At the CERES experiment, each electron/positron track is required to have a transverse momentum $p_\mathrm{T} > 0.2$ GeV, to fall into the rapidity interval $2.1 < \eta < 2.65$ in the lab frame and to have a pair opening angle $\Theta_{ee} > 35$ mrad. Finally, for comparison with the CERES data, eq. (5) has to be divided by $\mathrm{d}N/\mathrm{d}\eta$, the number of particles per unit rapidity. As the data have been taken close to midrapidity, *i.e.* around the central plateau of the approximate Gaussian distribution of $\mathrm{d}N/\mathrm{d}\eta$ in the c.m. frame as mentioned above, its value is assumed to be constant over the η range restricted by the detector cuts.

3 Spectrum above critical temperature

Lattice QCD calculations suggest [1–3] that sufficiently far above the critical temperature T_C for the deconfinement transition, quarks and gluons can be treated approximately as an ideal gas; they interact only weakly because of the behaviour of the running coupling strength α_s at high T. In this temperature region we can evaluate the hadronic part of the photon self-energy using perturbative QCD. To lowest order in α and to zeroth order in α_s, $\Pi_{\mu\nu}$ corresponds simply to the thermal quark-antiquark loop to which we restrict ourselves in the present paper. Higher-order thermal QCD corrections beyond the leading $q\bar{q}$ loop will be investigated in forthcoming work.

At our typical temperatures T of several hundred MeV, we need to take into account the three flavours u, d and s. Heavier quarks such as the c and b are strongly suppressed by Boltzmann factors because of their large mass and can be considered as "frozen". The total contribution to the dilepton emission rate is obtained by summing the individual $q\bar{q}$ contributions multiplied by the squares of the electric charges e_f of their respective flavour currents. In addition, each quark exists in three colours which leads to an overall multiplicative factor of $N_\mathrm{C} = 3$. Furthermore, the u and d quarks are considered massless and the heavier $s\bar{s}$-pair can only be produced if q^2 is larger than $4m_s^2$. So the total imaginary part of the self-energy which will be used in eq. (1), evaluated with standard finite-temperature techniques [19], is

$$\mathrm{Im}\bar{\Pi}(q,T) = \frac{q^2}{4\pi} \sum_{f=u,d,s} e_f^2 \; \theta(q^2 - 4m_f^2) \left(1 + \frac{2m_f^2}{q^2}\right) \times \sqrt{1 - \frac{4m_f^2}{q^2}} \left[\frac{2T}{|\mathbf{q}|} \left(1 - \frac{4m_f^2}{q^2}\right)^{-\frac{1}{2}} \ln \frac{f_D(E_-)}{f_D(E_+)} - 1\right], \qquad (6)$$

where

$$f_D(E) = \frac{1}{\exp(\beta E) + 1}$$

and

$$E_\pm = \frac{q^0}{2} \pm \frac{|\mathbf{q}|}{2}\sqrt{1 - \frac{4m_f^2}{q^2}}.$$

In the limit $T \to 0$, eq. (6) reduces to the well known vacuum result. At finite T, the quantity (6) is always smaller than $\mathrm{Im}\bar{\Pi}(q, T = 0)$ as a consequence of Pauli blocking.

4 Spectrum below critical temperature

At $T < 150$ MeV, confinement sets in and the effective degrees of freedom of the QCD Hamiltonian are now colourless hadrons. The photon can directly couple to $J^P = 1^-$ states (the lowest "dipole" excitations of the QCD vacuum). In the energy region of interest, these particles are the ρ-, ω- and ϕ-mesons and multi-pion states carrying the same quantum numbers. Our next step is thus to connect the electromagnetic current-current correlation function with the currents generated by these mesons. We use an effective Lagrangian which approximates the $SU(3)$ flavour sector of QCD at low energies. The appropriate model for our purposes is the *improved Vector Meson Dominance* model combined with chiral dynamics of pions and kaons as described in [12].

Within this model, the following relation between the imaginary part of the irreducible photon self-energy $\mathrm{Im}\bar{\Pi}$ and the vector meson self-energies $\Pi_V(q)$ in vacuum can be derived:

$$\mathrm{Im}\bar{\Pi}(q) = \sum_V \frac{\mathrm{Im}\Pi_V(q)}{g_V^2}\ |F_V(q)|^2, \tag{7}$$

$$F_V(q) = \frac{\left(1 - \frac{g}{g_V^0}\right) q^2 - m_V^2}{q^2 - m_V^2 + i\mathrm{Im}\Pi_V(p)}, \tag{8}$$

where m_V are the (renormalized) vector meson masses[1], g_V^0 is the γV coupling and g the ΦV coupling, where Φ stands for one of the pseudoscalar Goldstone bosons $\pi^\pm, \pi^0$ and $K^\pm, K^0$. Equation (7) is valid for a virtual photon with vanishing three-momentum, $q = (q^0, 0, 0, 0)$. Taking the limit $|\mathbf{q}| = 0$ should be reasonable for our purposes in view of the fact that the c.m. rapidity interval accessible at CERES restricts $|\mathbf{q}|$ on average to a fraction of the vector meson mass m_V. For finite three-momenta there would be two scalar functions $\bar{\Pi}_\mathrm{L}$ and $\bar{\Pi}_\mathrm{T}$, because the existence of a preferred frame of reference (the heat bath) breaks Lorentz invariance. In the following, we calculate the hadronic spectra Π_V at finite temperature.

4.1 The ρ-meson spectrum

The main decay channel of the ρ-meson is $\rho \to \pi^+\pi^-$ with a vacuum width $\Gamma \simeq 150$ MeV. In the VMD model, hadronic current conservation leads to two possibilities to couple ρ to pions: There is a pion tadpole diagram and a two-pion loop diagram. Both terms contribute to Π_ρ and correspondingly modify the ρ-meson properties. Their vacuum values are well known [12], thus in the following we will calculate only the changes induced by finite temperature.

Using the real-time formalism of thermal field theory [19], we find for the imaginary part of the two-pion loop diagram

$$\mathrm{Im}\bar{\Pi}(q^0, \mathbf{q} = 0) = -(q^0)^2 \frac{g_{\rho\pi\pi}^2}{48\pi}\left(1 - \frac{4m_\pi^2}{(q^0)^2}\right)^{\frac{3}{2}} \times \left(1 + 2f_B(q^0/2)\right)\theta(q^0 - 2m_\pi). \tag{9}$$

This is exactly the $T = 0$ result multiplied by the characteristic thermal factors: the imaginary part is larger than at zero temperature as a consequence of the Bose-enhancement of the thermal pions. Using the relation $\mathrm{Im}\bar{\Pi}(m_\rho) = m_\rho\Gamma$, we see that the decay width $\Gamma_{\rho\to\pi\pi}$ of the ρ-meson is enhanced because there are already thermally excited pions present in the heat bath. At temperatures of about 100 MeV, this effect causes an increase of the ρ width by about 20% . Additional sources of thermal broadening at high temperatures are reactions of the ρ-meson with pions in the heat bath, such as $\rho\pi \to 3\pi$. We checked that this is only a small correction to the width. Other decay modes of the ρ like $\rho \to \pi^+\pi^-\gamma$, not taken into account, may also start to play a role at high T, however, their branching ratios are very small.

The calculation of the real part of the thermal ρ-meson self-energy is technically more involved, but the resulting temperature dependent mass shift $\delta m_\rho(T)$ is small. Eletsky and Ioffe [20,21] have pointed out that the leading term of δm_ρ starts at order T^4 when ρ-a_1 mixing is properly taken into account. The actual evaluation of δm_ρ gives an (upward) mass shift of less than 3% of m_ρ even at temperatures as high as 150 MeV. We can therefore safely neglect this effect in our calculation.

Note that the general form of the thermal ρ spectrum does not change dramatically, at least up to $T \leq 150$ MeV. Substantial broadening of the ρ-meson spectrum is expected in the presence of large baryon density [12, 13]. However, under the conditions of Pb-Au collisions at CERN, the fireball rapidly expands and the baryon density at hadronization drops to a fraction of normal nuclear matter density. We can thus ignore such density effects.

4.2 The ω-meson spectrum

The main decay mode of the $\omega(783)$ vector meson with a branching ratio of 89% is $\omega \to \pi^+\pi^0\pi^-$ and $\Gamma_{\omega\to3\pi} = 7.5$ MeV. It is well known that a point-like coupling $\omega \to 3\pi$ does not describe the ω-decay properly. It is necessary to include an intermediate step, the Gell-Mann, Sharp, Wagner (GSW) process [22] $\omega \to \rho\pi \to \pi^+\pi^-\pi^0$. The full decay process is described by an interference between the amplitudes of these two processes. In the following, we

[1] In the present context, m_V is understood to include the shift from bare to physical mass induced by $\mathrm{Re}\Pi_V$ [12].

assume that the intermediate virtual ρ-meson propagation is merely a "vertex" correction and that the effects of temperature on the ρ-meson are small, so we can neglect them to leading order. This is justified by noting that the thermal production of a ρ-meson is heavily suppressed by $e^{-m_\rho/T} \ll 1$ in the temperature range we are interested in (up to about 150 MeV).

The explicit calculation [23] for an ω-meson at rest, $q_\omega = (\omega, \mathbf{q} = 0)$, leads us to the result

$$\mathrm{Im}\bar{\Pi}(\omega) = \frac{1}{192\pi^3}\left(\mathcal{B}_1 + 3\ \mathcal{B}_2\right), \tag{10}$$

$$\mathcal{B}_1 = \int_{\Delta_1} \mathrm{d}E_+ \mathrm{d}E_- \left(\mathbf{q}_+^2 \mathbf{q}_-^{\,2} - (\mathbf{q}_+ \times \mathbf{q}_-)^2\right) \times |\mathcal{M}(\omega; q_+, q_0, q_-)|^2 \times n(E_+, E_-, \omega),$$

$$\mathcal{B}_2 = -\int_{\Delta_2} \mathrm{d}E_+ \mathrm{d}E_- \left(\mathbf{q}_+^2 \mathbf{q}_-^{\,2} - (\mathbf{q}_+ \times \mathbf{q}_-)^2\right) \times |\mathcal{M}(\omega; q_+, -q_0, q_-)|^2 \times n(E_+, E_-, \omega),$$

where

$$\mathcal{M}(\omega; q_+, q_0, q_-) = \frac{-3h}{f_\pi^3} + 2\ \frac{g_{VVP}}{f_\pi}\ g_{\rho\pi\pi} \times \sum_{\alpha=+,0,-} \frac{1}{(q_\omega - q_\alpha)^2 - m_\rho^2 - \bar{\Pi}_\rho(q_\omega - q_\alpha)}.$$

Here, $\bar{\Pi}_\rho$ is the zero-temperature ρ-meson self-energy. Its explicit expression and a general discussion of this matrix element can be found in [12], including the coupling constants h and g_{VVP} (f_π is the pion decay constant). $E_\pm$ and $\mathbf{q}_\pm$ are the energies and momenta of the charged pions in the final state. To keep our notation short, we have introduced the function

$$n(E_+, E_-, \omega) = \Big((1 + f_B(E_+)) \times (1 + f_B(E_-))(1 + f_B(\omega - E_+ - E_-)) - f_B(E_+)\ f_B(E_-)\ f_B(\omega - E_+ - E_-)\Big).$$

In eq. (10), $\mathcal{B}_1$ describes the process of a Bose-enhanced three-particle decay of the ω-meson, $n(E_+, E_-, \omega)$ accounts for the characteristic Bose factors. The kinematically allowed integration region in the E_+E_- plane, Δ_1, is the same as in the $T = 0$ case for the decay process. It is limited to $m_\pi \le E_\pm \le \omega - 2m_\pi$ and $2m_\pi \le E_+ + E_- \le \omega - m_\pi$ with the constraint $\mathbf{q}_+^2 \mathbf{q}_-^{\,2} - (\mathbf{q}_+ \times \mathbf{q}_-)^2 > 0$.

To interpret the $\mathcal{B}_2$ term in eq. (10), we note that

$$-n(E_+, E_-, \omega) = \Big((1 + f_B(E_+)) \times (1 + f_B(E_-))\ f_B(E_+ + E_- - \omega) - f_B(E_+)\ f_B(E_-)\ (1 + f_B(E_+ + E_- - \omega))\Big), \tag{11}$$

by using $1 + f_B(E) + f_B(-E) = 0$. Thus $\mathcal{B}_2$ corresponds to the scattering of the ω-meson off a thermally excited π^0 into π^+ and π^-, where each particle has the characteristic thermal corrections. The integration region Δ_2 is still constrained by $\mathbf{q}_+^2 \mathbf{q}_-^{\,2} - (\mathbf{q}_+ \times \mathbf{q}_-)^2 > 0$, but now in the region defined by $E_+ + E_- \ge \omega + m_\pi$. Because the integration region Δ_2 is now unbounded and the functions involved are only damped by Bose factors and their combinations, the $\omega\pi \to \pi\pi$ scattering contribution to the decay width increases quite strongly with temperature, as we will see below. The factor 3 multiplying $\mathcal{B}_2$ comes from summing over all possible charge combinations $\omega + \pi^+ \to \pi^0 + \pi^+$, $\omega + \pi^- \to \pi^0 + \pi^-$ and $\omega + \pi^0 \to \pi^- + \pi^+$.

The evaluation of the real part of the ω-meson self-energy coupled to the 3π continuum is much more difficult than that of the imaginary part because it would involve a two-dimensional Cauchy principal-value integral. We refrain from calculating the real part of the three-body decay, assuming that its temperature dependent mass shift is not much different from the (small) one of the ρ-meson.

4.3 The ϕ-meson spectrum

Because of the large mass of the ϕ and its main two-body decays into heavy kaons, the impact of temperature on its spectrum is marginal. The thermal production of kaons at temperatures even as high as 150 MeV is still suppressed by an order of magnitude compared to thermal pion production. We find that the sharp peak structure of the ϕ-meson does not change as its total width increases by about 20% to just 5.2 MeV at the highest temperatures. Thus it is only moderately affected by temperature effects and one should be able to observe its sharp resonance structure in future dilepton rate measurements.

5 Integrated rates

Whereas the ρ- and ϕ-mesons experience only moderate thermal changes of their spectral functions, the ω spectrum changes its shape considerably, mainly due to $\omega\pi \to \pi\pi$ reactions in the heat bath. We now use eq. (7) to relate our temperature-dependent vector meson self-energies to the imaginary part of the electromagnetic current-current correlator which enters the dilepton rate formula (1) as long as we stay below T_C. Above this critical temperature, we use expression (6) which yields the dilepton emission rate from a thermal quark-antiquark system. It is instructive to have a look at the spin-averaged spectral distributions $R(q,T) = 12\pi\mathrm{Im}\bar{\Pi}(q,T)/q^2$ at different temperatures T (presented in fig. 1 for $q^\mu = (\omega, \mathbf{q} = 0)$).

Obviously, the spectral functions on either side of the quark-hadron transition are quite distinct: the $\mathrm{q\bar{q}}$ loop spectrum is flat with no significant structure whereas the hadronic spectra exhibit a clear resonance structure. How these differences manifest in the dilepton emission spectra is examined in this section where we convolute the dilepton rate with the space-time evolution of the fireball system to obtain the total rate (5) which can then be compared to the CERES/NA45 data.

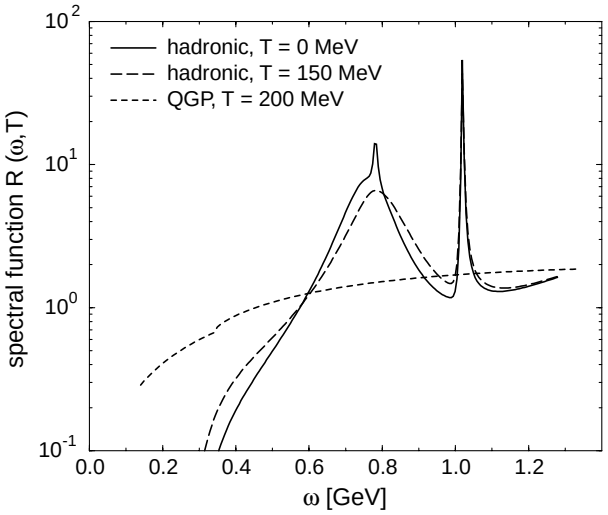

Fig. 1. Spectral distribution $R = 12\pi \mathrm{Im}\bar{\Pi}/q^2$ for $q^\mu = (\omega, \mathbf{q} = 0)$ for different temperatures above and below the quark-hadron transition. The background contribution to the hadronic spectra at large ω arises from the 4π continuum.

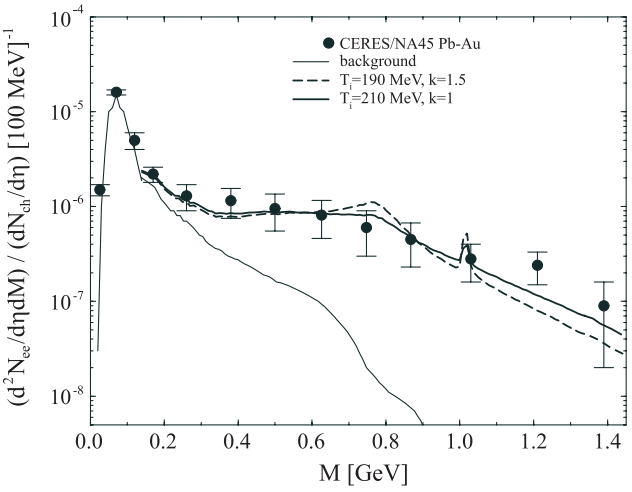

Fig. 2. Dilepton rates as a function of the invariant e^+e^- mass M, calculated in a mixed scenario (hadrons below T_C, quarks above $T_\mathrm{C} = 150$ MeV) for the Pb-Au case with two different initial temperatures. The background at low energies consists mainly of π^0, η and ω Dalitz decays. The data are taken from [7].

For a start, we use the parameters shown in table 1 for eqs. (3) and (4) which are adapted to reproduce the results of microscopic transport calculations [17,18] for the space-time evolution of the S-Au and Pb-Au collision (we show the Pb-Au parameters as this is the case of primary interest). Let us now apply our "mixed" model scenario (hadronic degrees of freedom below T_C, quarks above T_C) with $T_\mathrm{C} = 150$ MeV and initial temperatures of 190 MeV and 210 MeV, respectively. These two cases are shown in fig. 2. For the moment, we employ a direct transition between the two phases at T_C and comment on the implications of a possible mixed phase later.

We find that we can reproduce the shape of the data quite well. We need a normalization factor k which can be explained as follows: for the hadronic phase where thermal $\pi\pi$ annihilation is dominant, there is an increased population of the pion phase space due to a finite pion chemical potential we did not include [13]. However, the striking feature is that when choosing a higher initial temperature, $T^i = 210$ MeV, the normalization factor needed to reproduce the data becomes smaller, consistent with the picture that the system now stays for almost the whole expansion time in the partonic phase where there is no pionic chemical potential. We also checked that our calculations reproduce the observed transverse-momentum distributions: the main part of the enhancement resides in the $p_\mathrm{T} < 500$ MeV region.

We can therefore easily account for the dilepton "excess" in the intermediate mass region. At high masses, the scenario with $T^i = 190$ MeV still underestimates the data a bit. With a higher initial temperature $T^i = 210$ MeV, the slope becomes flatter and moves up in the right direction. This can be understood as follows: using a spin-averaged spectral function as in fig. 1, we can rewrite eq. (1) as

$$\frac{\mathrm{d}N}{\mathrm{d}^4x\ \mathrm{d}^4q} = \frac{\alpha^2}{12\pi^4} \cdot \frac{R(q^0, \mathbf{q})}{e^{\beta q^0} - 1}. \tag{12}$$

From eq. (6) it follows that the thermal spectrum R approaches its constant perturbative plateau for large momenta and high temperatures or for any momentum at low temperatures. From this we infer that in the QGP phase, the shape of the dilepton emission rate for high invariant mass at high T is basically determined by the inverse of the temperature, β, as

$$\frac{\mathrm{d}N}{\mathrm{d}^4x\ \mathrm{d}^4q} \sim \mathrm{const} \times e^{-\beta q^0}. \tag{13}$$

As the integrated rate (5) averages over all temperatures according to the fireball parametrization, we see in fig. 2 a straight fall-off at high invariant masses, with a slope

Table 1. Typical set of parameters controlling the space-time evolution of the fireball, adapted for the Pb-Au collisions at CERN-SPS. Baryon densities are given in units of $\rho_0 = 0.17$ fm^{-3}.

	Pb-Au
T^i	190 MeV
T^∞	105 MeV
τ_1	10 fm
ρ^i	2.55 ρ_0
τ_2	6 fm
N_B	260
$\mathrm{d}N/\mathrm{d}\eta$	220
t_f	10 fm
T_f	136 MeV
ρ_f	0.48 ρ_0

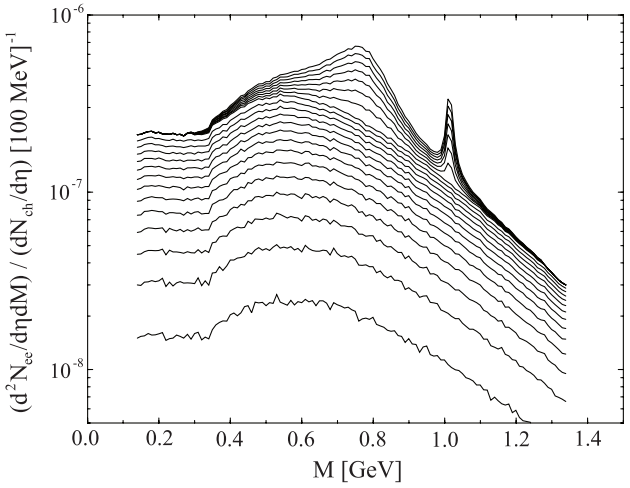

Fig. 3. A time snapshot of the Pb-Au fireball expansion with $T^i = 190$ MeV (no k factor). Shown are the integrated dilepton rates between the start of the expansion at $t = 0$ and the freeze-out time, $t_f = 10$ fm/c in steps of Δt =0.5 fm/c. The CERES acceptance is included. The different behaviour of the partonic and the hadronic phases below and above $T_C = 150$ MeV is clearly visible.

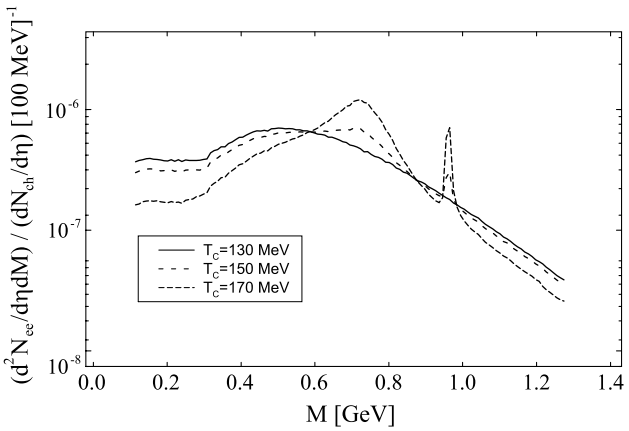

Fig. 4. The resulting Pb-Au dilepton emission spectra for three different critical temperatures, starting from the same initial temperature $T^i = 210$ MeV. For the sake of lucidity, the low-mass hadronic background has been omitted. No k factor has been applied.

parameter $-\langle 1/T \rangle$, averaged over the temperature evolution of the fireball. This is an important result: if we start with a different parametrization of the fireball, say, with a higher initial temperature, *the slope changes*, it becomes flatter because we average over $1/T$. Thus an accurate measurement of the dilepton rate at high invariant mass yields valuable information about the temperature evolution of the fireball, assuming that equilibration is fast.

In contrast to its appearance as a sharp resonance at $T = 0$, the ω-meson is hardly visible as a little bump on top of the broad ρ-meson spectrum. This was to be expected because the temperatures of the system in the hadronic phase before freeze-out are still quite high, between 150 and 125 MeV.

The ϕ-meson can still be identified as a sharp resonance. As the ϕ is hardly influenced by temperature, its height over background ratio may thus act as a chronometer for the critical time t_C once the fireball parameters are sufficiently well known: at $T^i = 210$ MeV, the ϕ-meson still sticks out of the QGP "background", but with a reduced height, confirming that the system stays now longer in the QGP phase than in the scenario with $T^i = 190$ MeV.

To get a better understanding for the space-time evolution of the fireball, let us look at the time snapshot picture of the fireball expansion in fig. 3. Shown are the integrated dilepton rates between the start of the expansion and the freeze-out time $t_f = 10$ fm/c in steps of $\Delta t = 0.5$ fm/c. Although the QGP phase is very hot in the beginning ($t_0 = 0$), its contribution to the dilepton rate is initially small because it occupies only a small volume. With the consecutive expansion, the rate per unit volume decreases as the temperature goes down. However, the increase in volume outweighs this effect partly. The shape of the spectrum stays roughly the same, but the slope for high M is now, following eq. (13), $-\beta\sqrt{M^2 + p_T^2}$ integrated over the transverse momentum p_T. The change in the slope with increasing time, or equivalently, with decreasing temperature is small yet visible, and the magnitude of the slope is set by the initial temperature.

At $t_C = 7$ fm/c, the phase transition occurs, the system goes into the hadronic phase and the ρ- and ϕ-meson resonances start to grow out of the QGP "background". It is clearly seen that the shape of the dilepton spectrum at high masses M is only determined by the QGP phase and that the ϕ-meson peak height would be larger if the transition occurred earlier or the freeze-out time were later.

With these observations in mind, we investigate the sensitivity of the spectra with respect to the parameters T_C and t_f. In fig. 4, the resulting Pb-Au dilepton emission spectra are shown for three different critical temperatures T_C =130, 150 and 170 MeV. The initial temperature is 210 MeV.

The slopes for high invariant mass M are equal in all three cases of T_C, as expected. For the lowest transition temperature, $T_C = 130$ MeV, we obtain a pure QGP spectrum. The higher T_C is chosen, the more "hadronic" the spectrum looks and the less dileptons are present in the intermediate mass range 0.3–0.6 GeV. At high T_C, the broad ρ-meson resonance sticks out clearly, so does the narrow ϕ-meson. From its peak height it is possible to judge how long the system has stayed in the hadronic phase before freeze-out. Note that the ω-meson is not visible even for high T_C, because of its increased thermal width. An amusing side note is that all three curves have four points in common, left and right to the resonances. We also checked that the *shape* of the dilepton rate is not sensitive to the freeze-out time.

So far, we have assumed that the transition from the QGP to the hadronic phase is instantaneous, in the sense that the quark phase at $T > T_C$ is separated from the hadron phase at $T < T_C$, and does not affect the time

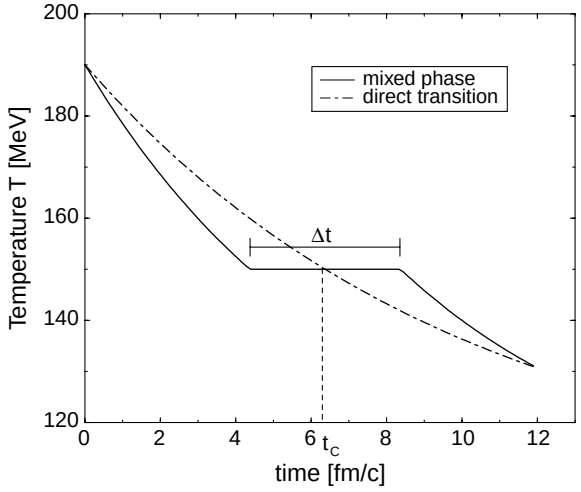

Fig. 5. Fireball temperature as a function of time for a direct transition and a possible mixed scenario.

evolution of temperature and volume. Exactly how the hadronization occurs is not known at this stage, but there are indications that it may actually extend over a finite time interval, during which a mixed phase prevails [24,25]. Lattice data show a discontinuity in the energy density at $T_{\rm C}$ [26], so this stage is accompanied by a release of latent heat. Such processes can imply that the temperature stays almost constant during the transition time which may be considerably long, of the order a few fm/c [27,28]. In order to estimate the consequences of these effects on the dilepton spectra, we have modified the time evolution of the fireball temperature such that there is a plateau of constant temperature $T_{\rm C}$, as shown in fig. 5. The width of the plateau is denoted by Δt, and the initial and freeze-out temperature are kept at the values listed in table 1.

During the transition, we assume that both phases exist in a homogeneous mixture and their relative occupation of the volume changes with time. Correspondingly, the spectral function entering the dilepton rates in eq. (12) is modified to

$$R(t) = \alpha(t) R_{QGP}(T_{\rm C}) + [1-\alpha(t)] R_{\rm hadr}(T_{\rm C}), \qquad (14)$$

where $\alpha(t_{\rm c} - \Delta t/2) = 1$, $\alpha(t_{\rm c} + \Delta t/2) = 0$ and between these limits α drops linearly. We found that even if Δt is set to a value as large as 5 fm/c, the difference in the dilepton rates is at most 40%. For $\Delta t = 1$ fm/c, the rates are virtually indistinguishable. Within the error bars of the data, we conclude that the existence of a mixed phase is neither confirmed nor excluded at the resolution currently available.

6 Conclusions

Within our simple fireball model, we can indeed reproduce the observed CERES dilepton spectra within a pure thermal model, assuming that there exists a partonic phase above a certain temperature $T_{\rm C}$. The transverse-momentum dependence is correctly described, too. With a sufficiently high initial temperature $T^i = 210$ MeV, the shape of the spectrum is perfectly well described. At such high initial temperatures, the system stays in the quark phase for much of its expansion period, and the dilepton radiation originates primarily from quark-antiquark annihilation, resulting in a flat spectrum. Hadronization in the final stage then leads to the appearance of resonance structures. We note that the thermal life time of the ω-meson may decrease such that the ω actually decays inside the fireball. The detailed shape of the spectra is sensitive to certain combinations of freeze-out, initial and critical temperature.

An improved experimental mass resolution in the region $M > 1$ GeV may yield important information about the initial temperature of the partonic phase. The role of the ϕ-meson as both a thermometer and a chronometer for the fireball expansion has been emphasized. Finally we investigated a possible mixed phase scenario and found that it would not leave any distinct traces in the shape of the dilepton rates.

This work has been supported in part by BMBF and GSI.

References

1. F. Karsch, *Proceedings of the International Workshop XXV on Gross Properties of Nuclei and Nuclear Excitations, Hirschegg, Austria, January 13-18, 1997* edited by H. Feldmeier, J. Knoll, W. Norenberg and J. Wambach (GSI, 1997), p. 458.
2. G. Boyd, S. Gupta, F. Karsch, E. Laermann, B. Peterson and K. Redlich, Phys. Lett. B **349**, 170 (1995).
3. C. Bernard et al., Phys. Rev. D **55**, 6861 (1997).
4. C. Bernard et al., Phys. Rev. D **45**, 3854 (1992).
5. Y. Iwasaki et al., Z. Phys. C **71**, 343 (1996).
6. F. Karsch, Nucl. Phys. Proc. Suppl. **83-84**, 14 (2000).
7. G. Agakichiev et al., CERES collaboration, Phys. Lett. B **422**, 405 (1998).
8. B. Lenkeit et al., Nucl. Phys. A **654**, 627c (1999).
9. R. Stock, Nucl. Phys. A **661**, 282 (1999).
10. G. Agakichiev et al., CERES collaboration, Phys. Rev. Lett. **75**, 1272 (1995).
11. R. Rapp, G. Chanfray and J. Wambach, Nucl. Phys. A **617**, 472 (1997).
12. F. Klingl, N. Kaiser and W. Weise, Z. Phys. A **356**, 193 (1996); Nucl. Phys. A **624**, 527 (1997).
13. R. Rapp and J. Wambach, Adv. Nucl. Phys. (in press), `hep-ph/9909229`, and references therein; W. Cassing and E.L. Bratkovskaya, Phys. Rep. **308**, 65 (1999).
14. K. Geiger, Phys. Rep. **258**, 237 (1995).
15. P. Braun-Munzinger, I. Heppe, J. Stachel, Phys. Lett. B **465**, 15 (1999).
16. D.K. Srivastava, `nucl-th/9903066`, subm. to Eur. Phys. J. C.
17. Q.G. Li, C.M. Ko and G.E. Brown, Phys. Rev. Lett. **75**, 4007 (1995); Nucl. Phys. A **606**, 568 (1996).
18. Q.G. Li, C.M. Ko, G.E. Brown and H. Sorge, Nucl. Phys. A **611**, 539 (1996).

19. M. Le Bellac, *Thermal Field Theory* (Cambridge University Press, 1996).
20. M. Dey, V.L. Eletsky and B.L. Ioffe, Phys. Lett. B **252**, 620 (1990).
21. V.L. Eletsky, Phys. Lett. B **245**, 229 (1990).
22. M. Gell-Mann, D. Sharp and W.E. Wagner, Phys. Rev. Lett. **8**, 261 (1952).
23. R.A. Schneider and W. Weise, preprint TUM/T39-00-13 (2000).
24. K. Rajagopal, Nucl. Phys. A **661**, 150 (1999).
25. K.S. Lee, M.J. Rhoades-Brown and U. Heinz, Phys. Rev. C **37**, 1452 (1988).
26. B. Beinlich, F. Karsch and A. Peikert, Phys. Lett. B **390**, (1997), 268.
27. H.W. Barz, B.L. Friman, J. Knoll and H. Schulz, Nucl. Phys. A **484**, 661 (1988).
28. E.E. Zabrodin, L.V. Bravina, L.P. Csernai, H. Stocker and W. Greiner, Phys. Lett. B **423**, 373 (1998).